

# Measurement of the decay rate of $\Xi_c^0 \rightarrow pK^-K^-\pi^+$ relative to $\Xi_c^0 \rightarrow \Xi^-\pi^+$

I. Danko,<sup>1</sup> D. Cronin-Hennessy,<sup>2</sup> C. S. Park,<sup>2</sup> W. Park,<sup>2</sup> J. B. Thayer,<sup>2</sup> E. H. Thorndike,<sup>2</sup>  
 T. E. Coan,<sup>3</sup> Y. S. Gao,<sup>3</sup> F. Liu,<sup>3</sup> R. Stroynowski,<sup>3</sup> M. Artuso,<sup>4</sup> C. Boulahouache,<sup>4</sup>  
 S. Blusk,<sup>4</sup> E. Dambasuren,<sup>4</sup> O. Dorjkhaidav,<sup>4</sup> R. Mountain,<sup>4</sup> H. Muramatsu,<sup>4</sup>  
 R. Nandakumar,<sup>4</sup> T. Skwarnicki,<sup>4</sup> S. Stone,<sup>4</sup> J.C. Wang,<sup>4</sup> A. H. Mahmood,<sup>5</sup> S. E. Csorna,<sup>6</sup>  
 G. Bonvicini,<sup>7</sup> D. Cinabro,<sup>7</sup> M. Dubrovin,<sup>7</sup> A. Bornheim,<sup>8</sup> E. Lipeles,<sup>8</sup> S. P. Pappas,<sup>8</sup>  
 A. Shapiro,<sup>8</sup> W. M. Sun,<sup>8</sup> A. J. Weinstein,<sup>8</sup> R. A. Briere,<sup>9</sup> G. P. Chen,<sup>9</sup> T. Ferguson,<sup>9</sup>  
 G. Tatishvili,<sup>9</sup> H. Vogel,<sup>9</sup> M. E. Watkins,<sup>9</sup> N. E. Adam,<sup>10</sup> J. P. Alexander,<sup>10</sup>  
 K. Berkelman,<sup>10</sup> V. Boisvert,<sup>10</sup> D. G. Cassel,<sup>10</sup> J. E. Duboscq,<sup>10</sup> K. M. Ecklund,<sup>10</sup>  
 R. Ehrlich,<sup>10</sup> R. S. Galik,<sup>10</sup> L. Gibbons,<sup>10</sup> B. Gittelman,<sup>10</sup> S. W. Gray,<sup>10</sup> D. L. Hartill,<sup>10</sup>  
 B. K. Heltsley,<sup>10</sup> L. Hsu,<sup>10</sup> C. D. Jones,<sup>10</sup> J. Kandaswamy,<sup>10</sup> D. L. Kreinick,<sup>10</sup>  
 V. E. Kuznetsov,<sup>10</sup> A. Magerkurth,<sup>10</sup> H. Mahlke-Krüger,<sup>10</sup> T. O. Meyer,<sup>10</sup>  
 N. B. Mistry,<sup>10</sup> J. R. Patterson,<sup>10</sup> T. K. Pedlar,<sup>10</sup> D. Peterson,<sup>10</sup> J. Pivarski,<sup>10</sup>  
 S. J. Richichi,<sup>10</sup> D. Riley,<sup>10</sup> A. J. Sadoff,<sup>10</sup> H. Schwarthoff,<sup>10</sup> M. R. Shepherd,<sup>10</sup>  
 J. G. Thayer,<sup>10</sup> D. Urner,<sup>10</sup> T. Wilksen,<sup>10</sup> A. Warburton,<sup>10</sup> M. Weinberger,<sup>10</sup>  
 S. B. Athar,<sup>11</sup> P. Avery,<sup>11</sup> L. Brevi-Newell,<sup>11</sup> V. Potlia,<sup>11</sup> H. Stoeck,<sup>11</sup> J. Yelton,<sup>11</sup>  
 B. I. Eisenstein,<sup>12</sup> G. D. Gollin,<sup>12</sup> I. Karliner,<sup>12</sup> N. Lowrey,<sup>12</sup> C. Plager,<sup>12</sup> C. Sedlack,<sup>12</sup>  
 M. Selen,<sup>12</sup> J. J. Thaler,<sup>12</sup> J. Williams,<sup>12</sup> K. W. Edwards,<sup>13</sup> D. Besson,<sup>14</sup> K. Y. Gao,<sup>15</sup>  
 D. T. Gong,<sup>15</sup> Y. Kubota,<sup>15</sup> S. Z. Li,<sup>15</sup> R. Poling,<sup>15</sup> A. W. Scott,<sup>15</sup> A. Smith,<sup>15</sup>  
 C. J. Stepaniak,<sup>15</sup> J. Urheim,<sup>15</sup> Z. Metreveli,<sup>16</sup> K. K. Seth,<sup>16</sup> A. Tomaradze,<sup>16</sup>  
 P. Zweber,<sup>16</sup> J. Ernst,<sup>17</sup> K. Arms,<sup>18</sup> E. Eckhart,<sup>18</sup> K. K. Gan,<sup>18</sup> C. Gwon,<sup>18</sup> H. Severini,<sup>19</sup>  
 P. Skubic,<sup>19</sup> S. A. Dytman,<sup>20</sup> J. A. Mueller,<sup>20</sup> S. Nam,<sup>20</sup> V. Savinov,<sup>20</sup> G. S. Huang,<sup>21</sup>  
 D. H. Miller,<sup>21</sup> V. Pavlunin,<sup>21</sup> B. Sanghi,<sup>21</sup> E. I. Shibata,<sup>21</sup> and I. P. J. Shipsey<sup>21</sup>

(CLEO Collaboration)

<sup>1</sup>*Rensselaer Polytechnic Institute, Troy, New York 12180*

<sup>2</sup>*University of Rochester, Rochester, New York 14627*

<sup>3</sup>*Southern Methodist University, Dallas, Texas 75275*

<sup>4</sup>*Syracuse University, Syracuse, New York 13244*

<sup>5</sup>*University of Texas - Pan American, Edinburg, Texas 78539*

<sup>6</sup>*Vanderbilt University, Nashville, Tennessee 37235*

<sup>7</sup>*Wayne State University, Detroit, Michigan 48202*

<sup>8</sup>*California Institute of Technology, Pasadena, California 91125*

<sup>9</sup>*Carnegie Mellon University, Pittsburgh, Pennsylvania 15213*

<sup>10</sup>*Cornell University, Ithaca, New York 14853*

<sup>11</sup>*University of Florida, Gainesville, Florida 32611*

<sup>12</sup>*University of Illinois, Urbana-Champaign, Illinois 61801*

<sup>13</sup>*Carleton University, Ottawa, Ontario, Canada K1S 5B6  
and the Institute of Particle Physics, Canada*

<sup>14</sup>*University of Kansas, Lawrence, Kansas 66045*

<sup>15</sup>*University of Minnesota, Minneapolis, Minnesota 55455*

<sup>16</sup>*Northwestern University, Evanston, Illinois 60208*

<sup>17</sup>*State University of New York at Albany, Albany, New York 12222*

<sup>18</sup>*Ohio State University, Columbus, Ohio 43210*  
<sup>19</sup>*University of Oklahoma, Norman, Oklahoma 73019*  
<sup>20</sup>*University of Pittsburgh, Pittsburgh, Pennsylvania 15260*  
<sup>21</sup>*Purdue University, West Lafayette, Indiana 47907*  
(Dated: November 13, 2018)

## Abstract

Using the CLEOIII detector at CESR, we have measured the branching ratio of the decay  $\Xi_c^0 \rightarrow pK^-K^-\pi^+$  relative to  $\Xi_c^0 \rightarrow \Xi^-\pi^+$ . We find  $\mathcal{B}(\Xi_c^0 \rightarrow pK^-K^-\pi^+)/\mathcal{B}(\Xi_c^0 \rightarrow \Xi^-\pi^+) = 0.35 \pm 0.06(\text{stat}) \pm 0.03(\text{syst})$ . In the resonant substructure of this mode, we find evidence for  $\Xi_c^0$  decays to  $p\overline{K}^*(892)^0K^-$ , and measure  $\mathcal{B}(\Xi_c^0 \rightarrow p\overline{K}^*(892)^0K^-) \cdot \mathcal{B}(\overline{K}^*(892)^0 \rightarrow K^-\pi^+)/\mathcal{B}(\Xi_c^0 \rightarrow \Xi^-\pi^+) = 0.14 \pm 0.03(\text{stat}) \pm 0.01(\text{syst})$  and  $\mathcal{B}(\Xi_c^0 \rightarrow pK^-K^-\pi^+)/\mathcal{B}(\Xi_c^0 \rightarrow \Xi^-\pi^+) = 0.21 \pm 0.04(\text{stat}) \pm 0.02(\text{syst})$  for the non- $\overline{K}^*(892)^0$   $\Xi_c^0 \rightarrow pK^-K^-\pi^+$  decays. This note has the revised numbers on the branching ratios with improved secondary vertex finding algorithm.

In the past decade, singly-charmed baryons (consisting of one heavy quark and two light quarks  $Qq_1q_2$ ) have been of interest to many phenomenologists working in the realm of Heavy Quark Effective Theory [1]. The heavy charm quark acts as a heavy nucleus and the light di-quark moves around it, analogous to the hydrogen atom. The CLEO experiment has discovered many new charmed baryons and measured their properties; in particular it has measured many of their relative branching fractions. The study of charmed baryon decays is complicated because they can proceed by three distinctly different processes; external  $W$ -emission, internal  $W$ -decay, and  $W$ -exchange. Disentangling the contributions of each of these processes requires the measurement of as many different decay modes as possible.

Improvements in the particle identification in the CLEO III [2] detector with the introduction of the RICH (Ring Imaging CHerenkov) sub-detector [3], have made it possible to search for decay modes previously contaminated by huge combinatorial background. This paper concentrates on one such decay mode of the  $\Xi_c^0$  (the  $csd$  charmed baryon, discovered by CLEO [4]), namely  $\Xi_c^0 \rightarrow pK^-K^-\pi^+$ , and its substructure. To measure the relative branching fractions we use  $\Xi_c^0 \rightarrow \Xi^-\pi^+$  as the normalizing mode. Charged conjugation is implied throughout the text. The only previous observation of the  $pK^-K^-\pi^+$  final state was made in 1990 by the ACCMOR Collaboration [5], who observed four  $\Xi_c^0 \rightarrow pK^-\bar{K}^*(892)^0$  decays; but there was no information on their rate.

The data for this analysis were collected using CLEO III detector based at the Cornell Electron Storage Ring (CESR) taken at and near the  $\Upsilon(2S)$ ,  $\Upsilon(3S)$ , and  $\Upsilon(4S)$  resonances. The integrated luminosity corresponds to  $7.2 \text{ fb}^{-1}$ . In the CLEO III detector configuration, the innermost tracking device is a four-layer double-sided silicon vertex detector surrounding the beam pipe. Beyond this vertex detector is the main cylindrical drift chamber [6], with the inner 16 layers being axial and the outer 31 layers having a small stereo angle. The tracking system is immersed in a 1.5 T solenoidal magnetic field and measures the momentum and specific ionization ( $dE/dx$ ) of charged particles. Outside the drift chamber is the RICH sub-detector [2] consisting of two concentric cylinders. The inner cylinder comprises LiF-crystal radiators on a carbon-fiber shell, while the outer one consists of thin multi-wire proportional chambers filled with a gas mixture of methane and TEA. Ultra-violet Cherenkov photons interact with the TEA emitting electrons that are multiplied by the chamber and whose image charge is sensed on pad detecting planes, thus localizing the photon positions. Between these two layers is a 16-cm thick gap which allows the Cherenkov cone to expand. Surrounding the RICH is the 7800 CsI crystal calorimeter for the identification of photons and electrons. Beyond the crystal calorimeter is the superconducting solenoid magnet and a muon detector system. The crystal calorimeter and the muon detectors are not used in this analysis.

To identify hadrons, we combine information on the specific ionization ( $dE/dx$ ) measured in the drift chamber and likelihoods obtained from the RICH detector. The RICH likelihood is formed for each hypothesis ( $i = \pi, K, p$ ) by using the measured positions of photons that are located within 3 standard deviations of their expected positions for the measured track momentum. The likelihood function for each particle hypothesis,  $i$ , is defined as,

$$L_i = \prod_{j=1}^{N^{obs}} [G(\theta_j^{obs} | \theta_i^{exp}) + B], \quad (1)$$

where  $G$  is a Gaussian-like probability function of observing the  $j^{th}$  photon at an angle  $\theta_j^{obs}$  with respect to the expected Cherenkov angle  $\theta_i^{exp}$  for particle type  $i$ , and  $B$  is a flat background probability function. The details of RICH identification are given elsewhere [7].

Similarly, using the  $dE/dx$  information, we construct a quantity for the different hypotheses ( $i = \pi, K, p$ ) as  $S_i$ , which is the difference between the measured and expected  $dE/dx$  for that hypothesis, expressed in units of its standard deviation. The RICH and  $dE/dx$  information for each pair of hypotheses is then combined to form  $\chi^2$  functions, for example,

$$\Delta\chi^2(p - \pi) = -2\log L_p + 2\log L_\pi + S_p^2 - S_\pi^2. \quad (2)$$

In this example real protons peak at negative values of  $\Delta\chi^2(p - \pi)$  whereas real pions tend to have positive values. If there is no RICH information available, or if the particle's momentum is less than 1.0 GeV/c (for a proton), or 0.5 GeV/c (for a kaon), we use only  $dE/dx$  information to form the  $\Delta\chi^2$  function.

All the primary charged tracks are required to have a distance of closest approach to the beam position in the  $\hat{r} - \hat{\phi}$  plane of less than 5 mm and of less than 5 cm along the  $\hat{z}$  axis. Typical beam dimension is 300 microns, 100 microns, and 10 mm in x, y, and z, respectively. In the CLEO environment charmed baryons do not have well separated decay vertices. We require that the scaled momentum of the charmed baryon candidate,  $x_p$ , be greater than 0.5. Here  $x_p = P/\sqrt{E_b^2 - M^2}$ ,  $P$  and  $M$  are the momentum and mass of the candidate, and  $E_b$  is the beam energy. This requirement dramatically suppresses combinatorial background, and dictates that the observed charmed baryons are the result of continuum production rather than from  $B$  meson decays.

Candidates for the  $\Xi_c^0 \rightarrow pK^-K^-\pi^+$  decay are reconstructed by combining one proton candidate, two kaon candidates, and a pion candidate. For the proton identification, we require  $\Delta\chi^2(p - K) < -4$  and  $\Delta\chi^2(p - \pi) < -4$ . Similarly for each kaon identification, we require  $\Delta\chi^2(K - p) < -4$  and  $\Delta\chi^2(K - \pi) < -4$ . Pions are selected with a loose  $dE/dx$  criteria  $|S_\pi| < 5$ . All charged tracks are required to have momenta in excess of 100 MeV/c. Once the four charged tracks are selected we kinematically constrain them to come from a common vertex. The invariant mass distribution of the  $pK^-K^-\pi^+$  candidates is shown in Fig. 1. The data are fit to a Gaussian signal function and a second-order polynomial background shape. The fit yields a signal of  $148 \pm 18$  events at a mass consistent with previous measurements of the  $\Xi_c^0$  [8] and a fitted width of  $4.1 \pm 0.5$  MeV/ $c^2$ , consistent with expected resolution of 4.5 MeV/ $c^2$  obtained using a GEANT-based Monte Carlo simulation [9].

In this multi-body final state,  $pK^-K^-\pi^+$ , we also search for resonant sub-structure  $\overline{K}^*(892)^0$  by calculating the invariant mass of each of the kaon candidates combined with the pion. Figure 2 shows the sideband-subtracted  $K^-\pi^+$  invariant mass using those  $pK^-K^-\pi^+$  combinations within 3 standard deviations of the  $\Xi_c^0$  mass peak. Candidates for the signal (sidebands) are selected within the mass region of 2458.3 – 2483.1 MeV/ $c^2$  (2417.6 – 2442.4 or 2498.3 – 2523.1 MeV/ $c^2$ ), as shown in Fig. 1. The low mass tail in this distribution is due to the fact that we combine both kaons with a pion. The correct combination appears in the peak region, and the incorrect one forms the low mass tail. This distribution is fit to the sum of two shapes. The first one is the  $\overline{K}^*(892)^0$  signal shape, which is generated using a 3-body phase space simulation of  $\Xi_c^0 \rightarrow pK^-\overline{K}^*(892)^0$ , with  $\overline{K}^*(892)^0 \rightarrow K^-\pi^+$ . For the second, we use a four-body non-resonant simulation of  $\Xi_c^0 \rightarrow pK^-K^-\pi^+$ , since the data show no evidence of any other narrow resonances. In particular, we also searched for the two-body decay of the  $\Xi_c^0 \rightarrow \Lambda(1520)\overline{K}^*(892)^0$ , where  $\Lambda(1520) \rightarrow pK^-$  and  $\overline{K}^*(892)^0 \rightarrow K^-\pi^+$ , and found no evidence for this mode. Moreover, broad resonances do not yield a statistically significant difference in shape than that from non-resonant production. We therefore model all the non- $\overline{K}^*(892)^0$  contributions using this non-resonant production model. We fit this plot to the sum of two shapes from Monte Carlo simulation, one obtained for non- $\overline{K}^*(892)^0$

$\Xi_c^0 \rightarrow pK^-K^-\pi^+$  decays (dashed histogram), and the other for resonant  $\Xi_c^0 \rightarrow pK^-\overline{K}^*(892)^0$  decays (dotted histogram), where  $\overline{K}^*(892)^0 \rightarrow K^-\pi^+$ . In the fit the two normalizations are constrained to add to unity. The statistics are too poor to extract any possible interference effects in the invariant mass distribution, and is therefore not considered here. The measured resonant and non- $\overline{K}^*(892)^0$  fractions are found to be  $0.39 \pm 0.06(\text{stat})$  and  $0.61 \pm 0.06(\text{stat})$ , respectively. Thus, of the total  $148 \pm 18$  fitted  $\Xi_c^0 (\rightarrow pK^-K^-\pi^+)$  candidates  $58 \pm 11(\text{stat})$  events are contributed by resonant  $pK^-\overline{K}^*(892)^0$  decays and  $90 \pm 14(\text{stat})$  events are contributed by non- $\overline{K}^*(892)^0$  decays. The  $\chi^2/\text{dof}$  of the fit (shown in Fig. 2) to the resonant and non- $\overline{K}^*(892)^0$  components is found to be 44/45, indicating that our fitting function, which includes a contribution from only one resonance, is a satisfactory one within the available statistics, and we believe that the systematic uncertainty may be neglected.

The reconstruction efficiency of these two final states are estimated using the Monte Carlo simulation. Within the kinematic region  $x_p > 0.5$ , we find that both final states have a reconstruction efficiency of  $(23 \pm 1)\%$ . The corresponding efficiency-corrected measured cross-sections times branching fractions ( $\sigma \cdot \mathcal{B}$ ) are  $91 \pm 12(\text{stat}) \pm 8(\text{syst})$ ,  $37 \pm 7(\text{stat}) \pm 3(\text{syst})$ , and  $54 \pm 9(\text{stat}) \pm 5(\text{syst})$  fb for all  $pK^-K^-\pi^+$ ,  $\overline{K}^*(892)^0$  resonant ( $\overline{K}^*(892)^0 \rightarrow K^-\pi^+$  only) and non- $\overline{K}^*(892)^0$   $pK^-K^-\pi^+$ , respectively, where all the measurements refer to that part of the momentum spectrum with  $x_p > 0.5$ .

As the production cross-section of  $\Xi_c^0$  baryons is unknown, we do not have a measure of the absolute branching fraction of any  $\Xi_c^0$  mode. Instead, we measure the branching ratios of these new modes with respect to that of the well-established decay  $\Xi_c^0 \rightarrow \Xi^-\pi^+$ , where  $\Xi^- \rightarrow \Lambda\pi^-$ . Both the  $\Xi^-$  and its daughter  $\Lambda$  have long flight paths, with  $c\tau$  values of 4.91 and 7.89 cm, respectively. Therefore, in the  $\Xi_c^0 \rightarrow \Xi^-\pi^+$  decay chain we have two vertices significantly detached from the beamspot. The  $\Lambda$  sample is selected by vertexing two oppositely charged tracks. The protons from the  $\Lambda$  decays, which have the higher momentum of the two daughters, are required to be consistent with a proton hypothesis ( $\Delta\chi^2(p-K)$  and  $\Delta\chi^2(p-\pi) < 0$ ). Background is further rejected by requiring the daughter tracks from the  $\Lambda$  to be inconsistent with coming from the beam interaction point. The  $\Lambda$  candidates within 5 MeV/ $c^2$  (3 standard deviations) of the nominal PDG [8] mass (1115.68 MeV/ $c^2$ ) are then kinematically constrained to this mass and combined with an appropriately charged track to form the  $\Xi^-$  candidate. The  $\Lambda$  decay vertex is required to be at a greater distance from the beamspot than the  $\Xi^-$  decay vertex. The  $\Xi^-$  candidates are also required to have a flight distance of 3 mm or more before decaying. Pions from the  $\Xi^-$  baryons are required not to come from the interaction point, by requiring the  $\chi^2$  of the fit (if forced to come from the interaction point) to be greater than 3. Those  $\Xi^-$  candidates within 7 MeV/ $c^2$  (3 standard deviations) of the PDG [8] mass (1321.31 MeV/ $c^2$ ) are kinematically constrained to this mass and are used for further analysis. Finally a charged track consistent with the pion hypothesis is combined with the  $\Xi^-$  candidate to reconstruct the  $\Xi_c^0$  candidate. A fit to the  $\Xi^-\pi^+$  invariant mass distribution returns a signal yield of  $182 \pm 18$  and a mass consistent with previous measurements as shown in Fig. 3. The  $\Xi_c^0 \rightarrow \Xi^-\pi^+$  reconstruction efficiency is measured to be  $(9.8 \pm 0.3)\%$ . The measured branching fraction times the cross section ( $\sigma \cdot \mathcal{B}$ ) for the  $\Xi^-\pi^+$  mode is  $260 \pm 26(\text{stat}) \pm 23(\text{syst})$  fb for  $x_p > 0.5$ .

The measured relative branching fractions of the  $\Xi_c^0 \rightarrow pK^-K^-\pi^+$  modes are tabulated in Table I.

We investigated several sources of uncertainty, including background shapes, signal width, Monte Carlo statistics, charged particle identification, and  $\Lambda$  and  $\Xi^-$  reconstruction. The dominant uncertainties arise from the  $\Xi^-\pi^+$  mode, due to the reconstruction of the displaced

TABLE I: Measured branching fractions of the  $\Xi_c^0 \rightarrow pK^-K^-\pi^+$  mode relative to that for  $\Xi_c^0 \rightarrow \Xi^-\pi^+$ . The errors after the values give the statistical and systematic uncertainties, respectively.

Ratio of modes	Relative branching fraction
$\frac{\mathcal{B}(\Xi_c^0 \rightarrow pK^-K^-\pi^+)}{\mathcal{B}(\Xi_c^0 \rightarrow \Xi^-\pi^+)}$	$0.35 \pm 0.06 \pm 0.03$
$\frac{\mathcal{B}(\Xi_c^0 \rightarrow pK^-\overline{K}^*(892)^0) \cdot \mathcal{B}(\overline{K}^*(892)^0 \rightarrow K^-\pi^+)}{\mathcal{B}(\Xi_c^0 \rightarrow \Xi^-\pi^+)}$	$0.14 \pm 0.03 \pm 0.01$
$\frac{\mathcal{B}(\Xi_c^0 \rightarrow pK^-K^-\pi^+)_{\text{No } \overline{K}^*(892)^0}}{\mathcal{B}(\Xi_c^0 \rightarrow \Xi^-\pi^+)}$	$0.21 \pm 0.04 \pm 0.02$

vertices.

To estimate the uncertainty due to our assumptions in the shape of the background, we tried both first and second order polynomials to describe its shape. The fitted yield changed by 3%, which we take as our systematic uncertainty from this source. The systematic uncertainty due to the imperfect understanding of the signal resolution is taken as the difference in  $\Xi_c^0$  signal yield using a floating width and a width fixed to the value found from simulation (3% for the branching ratios, 6% and 8% for the  $pK^-K^-\pi^+$  and the  $\Xi^-\pi^+$  modes, respectively). We assign 4% and 5% systematic uncertainties to the  $\Xi_c^0 \rightarrow pK^-K^-\pi^+$  and  $\Xi_c^0 \rightarrow \Xi^-\pi^+$  decay modes, respectively, due to the finite statistics of the Monte Carlo samples. As the number of tracks for the observed (numerator) and the normalizing (denominator) modes are the same, the 1% per track uncertainty in basic track-finding cancels in the calculation of the branching ratio, as does the uncertainty in the luminosity (2%). Systematic uncertainties in the charged particle identification are investigated using samples of protons and kaons from the  $\Lambda \rightarrow p\pi^-$  and  $\Lambda_c \rightarrow pK^-\pi^+$  modes, respectively. The study demonstrated that the uncertainties in the particle identification for protons and kaons in the relevant momentum range are 3.2% and 2.4%, respectively. As there are two kaons in the final state, we assign 4.8% uncertainty to the kaon identification. Based on a study of displaced vertex finding in data and Monte Carlo we assign systematic uncertainties of 6% to the  $\Lambda$  finding and 2.8% to the  $\Xi^-$  finding; these numbers include the extra uncertainty in track-finding for low momentum, large impact parameter tracks. All systematic uncertainties are summarized in Table II. The total systematic uncertainty, obtained by adding the individual contributions in quadrature, is 9%, and considerably less than the statistical uncertainty.

In conclusion, we have measured the branching fraction for  $\Xi_c^0 \rightarrow pK^-K^-\pi^+$  relative to  $\Xi_c^0 \rightarrow \Xi^-\pi^+$ . We find that  $39 \pm 6(\text{stat})\%$  of the signal proceeds via the resonance sub-structure  $pK^-\overline{K}^*(892)^0$ , where  $\overline{K}^*(892)^0 \rightarrow K^-\pi^+$  with the remainder being the non- $\overline{K}^*(892)^0$  decay  $pK^-K^-\pi^+$ . Results are given as a ratio normalized to the  $\Xi^-\pi^+$  rate. The measured branching ratios for  $\frac{\mathcal{B}(pK^-K^-\pi^+)}{\mathcal{B}(\Xi^-\pi^+)}$ ,  $\frac{\mathcal{B}(pK^-\overline{K}^*(892)^0) \cdot \mathcal{B}(\overline{K}^*(892)^0 \rightarrow K^-\pi^+)}{\mathcal{B}(\Xi^-\pi^+)}$ , and  $\frac{\mathcal{B}(pK^-K^-\pi^+)_{\text{No } \overline{K}^*(892)^0}}{\mathcal{B}(\Xi^-\pi^+)}$  are  $0.35 \pm 0.06(\text{stat}) \pm 0.03(\text{syst})$ ,  $0.14 \pm 0.03(\text{stat}) \pm 0.01(\text{syst})$ , and  $0.21 \pm 0.04(\text{stat}) \pm 0.02(\text{syst})$ , respectively. This is the first measurement of a  $\Xi_c^0$  decay mode where both of the  $s$  quarks in the final state are part of mesons. It is possible that such four-body decays proceed via external  $W$ -decay, internal  $W$ -decay or  $W$ -exchange decay diagrams. Resonant decays such as  $p\overline{K}^*(892)^0K^-$ , which have no  $\pi^+$  in the final state, cannot decay via external  $W$ -decay. Their observation is not surprising, as many such

TABLE II: Systematic Uncertainties: The systematic errors listed under Ratio are for the relative branching fractions and the errors tabulated in the third and fourth column are  $pK^-K^-\pi^+$  and  $\Xi^-\pi^+$  modes, respectively.

Source	Uncertainty (%)		
	Ratio	$pK^-K^-\pi^+$	$\Xi^-\pi^+$
Luminosity	-	2	2
Track Reconstruction	-	4	4
Background shape	3	3	3
Signal Width (Monte Carlo)	3	6	8
$pK^-K^-\pi^+$ (Monte Carlo statistics)	4	4	-
$\Xi^-\pi^+$ (Monte Carlo statistics)	5	-	5
Proton ID	3.2	3.2	3.2
Kaon ID (two kaons)	4.8	4.8	-
$\Lambda$ reconstruction	6	-	6
$\Xi^-$ reconstruction	2.8	-	2.8
Total	9.8	9	9

$\Lambda_c^+$  and  $\Xi_c^0$  decays modes have been discovered, and is a further indication that external  $W$ -decay diagrams do not dominate in charmed baryon decays.

We gratefully acknowledge the effort of the CESR staff in providing us with excellent luminosity and running conditions. M. Selen thanks the Research Corporation, and A.H. Mahmood thanks the Texas Advanced Research Program. This work was supported by the National Science Foundation, and the U.S. Department of Energy.

- 
- [1] Yoji Kohara, Phys. Rev. D **44**, 2799 (1991); J.F. Donoghue, E. Golowich and, B.B Holstein, “Dynamics of the Standard Model”, Cambridge University Press (1994); J.G. Korner, in *Proceedings of the International Conference on The Structure of Baryons, Santa Fe, 1995*, edited by B.F. Gibson, P.D. Barnes, J.B. McClelland, and, W. Weise (World Scientific, Singapore, 1996), p. 221.
  - [2] CLEO Collaboration, S. Kopp *et al.*, Nucl. Instrum. Meth. A **384**, 61 (1996); A. Wolf *et al.*, Nucl. Instrum. Meth. A **408**, 58 (1998); G. Viehhauser *et al.*, Nucl. Instrum. Meth. A **462**, 146 (2001).
  - [3] CLEO Collaboration, R. Mountain *et al.*, Nucl. Instrum. Meth. A **433**, 77 (1999); M. Artuso *et al.*, Nucl. Instrum. Meth. A **502**, 91 (2003).
  - [4] P. Avery *et al.*, Phys. Rev. Lett. **62**, 683 (1989).
  - [5] ACCMOR Collaboration, S. Barlag *et al.*, Phys. Lett. B **236**, 495 (1990).
  - [6] CLEO Collaboration, D. Peterson *et al.*, Nucl. Instrum. Meth. A **478**, 142 (2002).
  - [7] CLEO Collaboration, D. Cronin-Hennessy *et al.*, Phys. Rev. D **67**, 012001 (2003).
  - [8] The Particle Data Group, A. Hagiwara *et al.*, Phys. Rev. D **66**, 010001 (2002).
  - [9] R. Brun *et al.*, CERN Report Number CERN-DD/EE84-1 (1987).

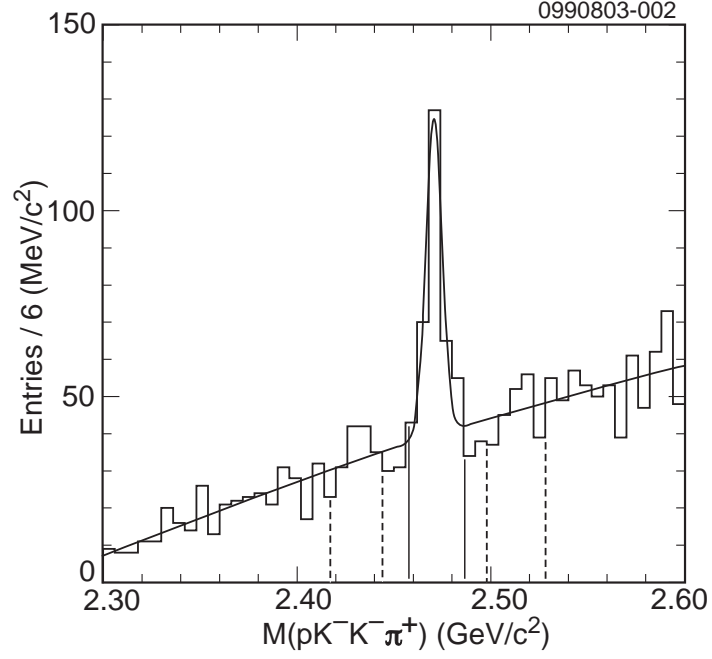


FIG. 1: Invariant mass distribution of  $pK^-K^-\pi^+$  candidates in CLEOIII data. The fit to the above mass distribution yields  $148 \pm 18$  signal events. The signal band ( $2458.3 - 2483.1 \text{ MeV}/c^2$ ) is defined within the solid lines and the low ( $2417.6 - 2442.4 \text{ MeV}/c^2$ ) and high ( $2498.3 - 2523.1 \text{ MeV}/c^2$ ) side bands are defined by the dashed lines.



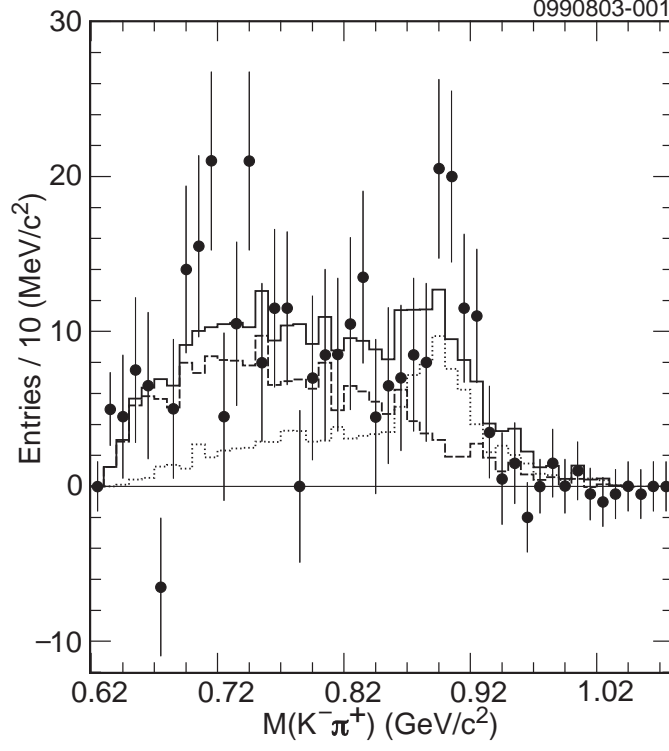


FIG. 2: The  $K^-\pi^+$  invariant mass in CLEO III data for  $\Xi_c^0$  candidates within 3 standard deviations of the PDG value. The two sideband contributions have been subtracted. Dots with error bars are data points, the dashed histogram is the non- $\bar{K}^*(892)^0$  contribution and the dotted histogram is the resonant contribution. The solid line histogram is the sum of the two contributions.

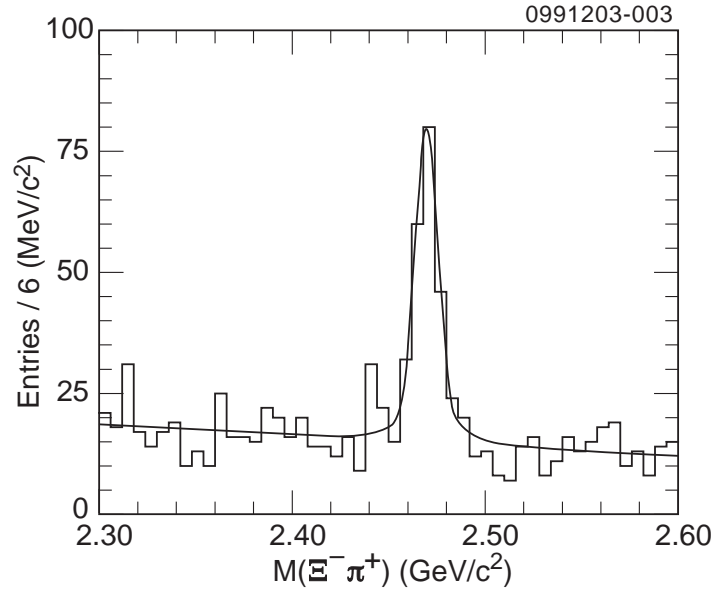


FIG. 3: Invariant mass distribution of  $\Xi_c^-\pi^+$  candidates in CLEO III data. The fit to the mass distribution yields  $182 \pm 18$  signal events and the fitted mean is consistent with the nominal  $\Xi_c^0$  PDG mass [8].